


 Cite this: *RSC Adv.*, 2020, 10, 30671

Reactions of triosmium and triruthenium clusters with 2-ethynylpyridine: new modes for alkyne C–C bond coupling and C–H bond activation†

 Md. Tuhinur R. Joy,^a Roknuzzaman,^a Md. Emdad Hossain,^a Shishir Ghosh,^a Derek A. Tocher,^b Michael G. Richmond^c and Shariff E. Kabir^{*a}

The reaction of the trimetallic clusters [H₂Os₃(CO)₁₀] and [Ru₃(CO)₁₀L₂] (L = CO, MeCN) with 2-ethynylpyridine has been investigated. Treatment of [H₂Os₃(CO)₁₀] with excess 2-ethynylpyridine affords [HOS₃(CO)₁₀(μ-C₅H₄NCH=CH)] (1), [HOS₃(CO)₉(μ₃-C₅H₄NC=CH₂)] (2), [HOS₃(CO)₉(μ₃-C₅H₄NC=CCO₂)] (3), and [HOS₃(CO)₁₀(μ-CH=CHC₅H₄N)] (4) formed through either the direct addition of the Os–H bond across the C≡C bond or acetylenic C–H bond activation of the 2-ethynylpyridine substrate. In contrast, the dominant pathway for the reaction between [Ru₃(CO)₁₂] and 2-ethynylpyridine is C–C bond coupling of the alkyne moiety to furnish the triruthenium clusters [Ru₃(CO)₇(μ-CO)(μ₃-C₅H₄NC=CHC(C₅H₄N)=CH)] (5) and [Ru₃(CO)₇(μ-CO)(μ₃-C₅H₄NCCHC(C₅H₄N)CHCHC(C₅H₄N))] (6). Cluster 5 contains a metalated 2-pyridyl-substituted diene while 6 exhibits a metalated 2-pyridyl-substituted triene moiety. The functionalized pyridyl ligands in 5 and 6 derive via the formal C–C bond coupling of two and three 2-ethynylpyridine molecules, respectively, and 5 and 6 provide evidence for facile alkyne insertion at ruthenium clusters. The solid-state structures of 1–3, 5, and 6 have been determined by single-crystal X-ray diffraction analyses, and the bonding in the product clusters has been investigated by DFT. In the case of 1, the computational results reveal a rare thermodynamic preference for a terminal hydride ligand as opposed to a hydride-bridged Os–Os bond (3c,2e Os–Os–H bond).

 Received 19th June 2020
 Accepted 29th July 2020

DOI: 10.1039/d0ra05393g

rsc.li/rsc-advances

1. Introduction

2-Vinylpyridine is well known for its ability to stabilize transition metal–carbon bonds in a chelating coordination mode.^{1–10} Early investigative work on the coordination chemistry of this ligand at mono- and polynuclear metal compounds has produced many excellent publications from the academic community.^{1–18} At mononuclear centers, coordination of this ligand occurs through the nitrogen donor of the pyridyl ligand, which in turn derives from the short-lived precursor involving the alkene functionality (π-complex). Once coordinated, the 2-vinylpyridine ligand is activated with respect to competitive C–H bond activation at the β-C–H alkenyl bond.^{1–10} In contrast,

many heterocyclic-substituted polynuclear clusters supporting a non-spectator nitrogen ligand have been isolated and structurally characterized using 2-vinylpyridine as a ligand. As part of our interest in the role played by metal cluster compounds in potential catalytic cycles, we continue to explore the reactivity pathways involving metal clusters and heterocyclic substrates. It should be noted that the majority of examples of metalated polynuclear derivatives derived from 2-vinylpyridine display common coordination modes for the heterocyclic auxiliary. This particular pyridyl ligand has been shown to coordinate up to four metal atoms and function as a 4e or 6e donor (Chart 1).^{11–18}

In comparison to the large number of reports on the reactivity of 2-vinylpyridine at metal clusters, fewer studies exist on the coordination chemistry of the acetylenic counterpart 2-ethynylpyridine at metal clusters.^{11,19,20} In 1985, a cooperative investigation on the reaction of [H₂Os₃(CO)₁₀] with 2-ethynylpyridine was conducted by the groups of Lewis, Hursthouse, and Deeming (LHD). The published report presented data for the existence of two products (Scheme 1), and the structure of one of the products (minor) was unequivocally established by X-ray crystallography. The solid-state structure of the minor product [HOS₃(CO)₁₀(μ-C₅H₄NCH=CH)] displays an opened triangular core with the ancillary pyridyl ligand functioning as a 5e donor that includes both nitrogen and (Z)-σ,π-alkenyl

^aDepartment of Chemistry, Jahangirnagar University, Savar, Dhaka 1342, Bangladesh. E-mail: sghosh_006@yahoo.com; skabir_ju@yahoo.com

^bDepartment of Chemistry, University College London, 20 Gordon Street, London WC1H 0AJ, UK

^cDepartment of Chemistry, University of North Texas, 1155 Union Circle, Box 305070, Denton, TX 76203, USA

 † Electronic supplementary information (ESI) available: IR and ¹H NMR spectral data on clusters 2, 3, 5, and 6. Atomic coordinates and energies for all DFT-optimized structures are available upon request (MGR). CCDC 2009586 (1), 2009587 (2), 2009588 (3), 2009591 (5), and 2009592 (6). For ESI and crystallographic data in CIF or other electronic format see DOI: 10.1039/d0ra05393g

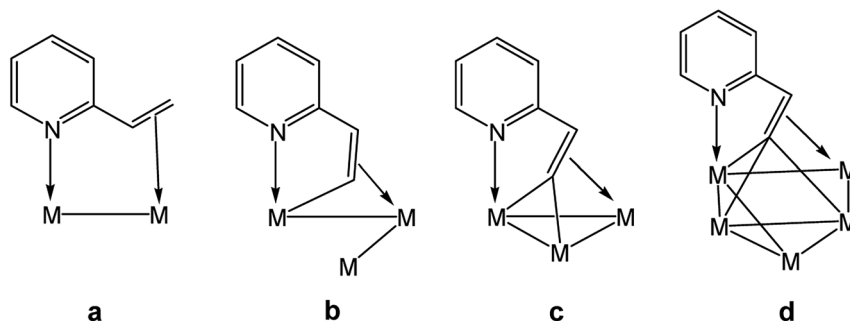
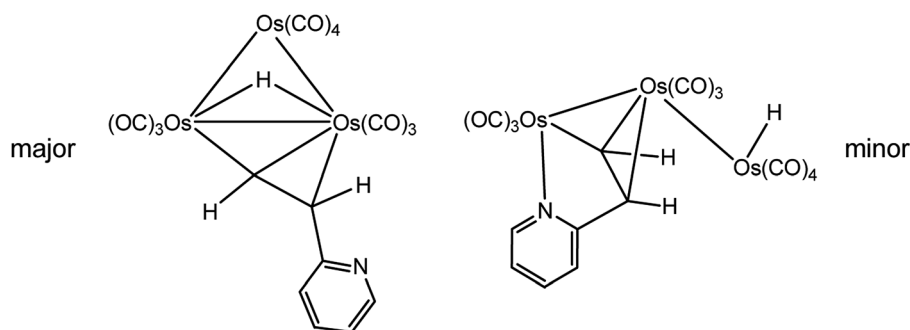



Chart 1 Known binding modes of non-metalated (a), mono-metalated (b), di-metalated (c), and tri-metalated (d) 2-vinylpyridine ligands at polynuclear transition metal centers.



Scheme 1 LHD major (left) and minor (right) products isolated from the reaction of $[\text{H}_2\text{Os}_3(\text{CO})_{10}]$ with 2-ethynylpyridine.¹¹

contributions.¹¹ The structure of the major isomeric product was formulated to have a dangling (free) pyridyl ligand with an (*E*)-alkenyl moiety that functions as a traditional σ,π -vinyl donor. The route that affords the major product was ascribed to an addition path involving an Os–H bond and the alkyne unit.

We have investigated the reactivity of different heterocycles containing a vinyl functionality at the *ortho* position such as 2-vinylpyridine, 2-vinylpyrazine, *etc.* at polynuclear metal centers over the last few years.^{16–18,20} Wishing to extend these studies based on alkenyl-substituted heterocyclic ligands, we have investigated the reaction of 2-ethynylpyridine with $[\text{Ru}_3(\text{CO})_{12}]$, which affords novel Ru_3 products based on C–C bond coupling of alkyne carbons of the pyridyl substrate. We have also reinvestigated the reaction of $[\text{H}_2\text{Os}_3(\text{CO})_{10}]$ with 2-ethynylpyridine and now report the isolation of two new cluster products 2 and 3 and confirm the unexpected isomerization of the major species found in the LHD study at elevated temperature to the minor isomer having an opened cluster polyhedron.¹¹

2. Experimental section

2.1. General remarks

All reactions were carried out under an inert atmosphere of nitrogen using standard Schlenk techniques unless otherwise stated. Reagent grade solvents were dried by standard methods and were freshly distilled prior to use. Infrared spectra were recorded on a Shimadzu IR Prestige-21 spectrophotometer, while the ^1H NMR spectra were recorded on a Bruker Advance III HD (400 MHz) instrument. All chemical shifts are reported in

δ units and are referenced to the residual protons of the deuterated solvent. Elemental analyses were performed by the Microanalytical Laboratories of the Wazed Miah Science Research Centre at Jahangirnagar University. $[\text{Os}_3(\text{CO})_{12}]$ and $[\text{Ru}_3(\text{CO})_{12}]$ were purchased from Strem Chemical Inc. and used without further purification. 2-Ethynylpyridine was purchased from Acros Organics and used as received. The starting clusters $[\text{H}_2\text{Os}_3(\text{CO})_{10}]$ ²¹ and $[\text{Ru}_3(\text{CO})_{10}(\text{NCMe})_2]$ ²² were prepared according to the published procedures. All products were separated in the air using preparative TLC plates coated with 0.25 mm of silica gel (HF254-type 60, E. Merck, Germany).

2.2. Reaction of $[\text{H}_2\text{Os}_3(\text{CO})_{10}]$ with 2-ethynylpyridine

A CH_2Cl_2 solution (15 mL) of $[\text{H}_2\text{Os}_3(\text{CO})_{10}]$ (50 mg, 0.059 mmol) and 2-ethynylpyridine (25 mg, 0.24 mmol) was stirred at room temperature for 15 min. The color of the reaction mixture changed from purple to orange by this time. The solvent was removed under reduced pressure and the residue purified by preparative TLC. Elution with cyclohexane/ CH_2Cl_2 (7 : 3 v/v) developed four bands which afforded the following compounds, in order of elution, yellow $[\text{HOs}_3(\text{CO})_{10}(\mu\text{-C}_5\text{H}_4\text{NCH}=\text{CH})]$ (1; LHD minor product; 14 mg, 25%), orange $[\text{HOs}_3(\text{CO})_9(\mu_3\text{-C}_5\text{H}_4\text{NC}=\text{CH}_2)]$ (2) (8.8 mg, 15%), orange $[\text{HOs}_3(\text{CO})_9(\mu_3\text{-C}_5\text{H}_4\text{NC}=\text{CCO}_2)]$ (3) (17 mg, 30%), and yellow $[\text{HOs}_3(\text{CO})_{10}(\mu\text{-CH}=\text{CHC}_5\text{H}_4\text{N})]$ (4; LHD major product; 11 mg, 20%). Data for 2: anal. calc. for $\text{C}_{16}\text{H}_7\text{NO}_9\text{Os}_3$: C, 20.71; H, 0.76; N, 1.51. Found: C, 20.98; H, 0.78; N, 1.55%. IR ($\nu(\text{CO})$, CH_2Cl_2): 2083s, 2051vs, 2028vs, 1995vs, 1983sh, 1970m,

1958 cm^{-1} . $^1\text{H NMR}$ (CDCl_3): δ 8.56 (d, J 6.0 Hz, 1H), 7.64 (m, 1H), 6.98 (m, 1H), 6.92 (d, J 8.0 Hz, 1H), 4.30 (s, 1H) 2.63 (s, 1H), -17.70 (s, 1H). Data for **3**: anal. calc. for $\text{C}_{17}\text{H}_5\text{NO}_{11}\text{Os}_3$: C, 21.05; H, 0.52; N, 1.44. Found: C, 21.23; H, 0.55; N, 1.51%. IR ($\nu(\text{CO})$, CH_2Cl_2): 2104m, 2079vs, 2060vs, 2025s, 2005m, 1990w, 1693w cm^{-1} . IR ($\nu(\text{CO})$, KBr): 2102m, 2075s, 2056s, 2033s, 2018s, 1996vs, 1979s, 1692w cm^{-1} . $^1\text{H NMR}$ (CDCl_3): δ 8.63 (d, J 6.0 Hz, 1H), 7.88 (m, 1H), 7.76 (d, J 8.0 Hz, 1H), 7.00 (m, 1H), -16.76 (s, 1H).

2.3. Isomerization of **4** to **1**

To a 5 mm NMR tube was charged cluster **4** (8.0 mg, 0.0080 mmol) and 0.75 mL of CDCl_3 . The tube was then placed in the NMR probe, and the progress of the isomerization was monitored at 60 °C. Quantitative conversion to **1** was confirmed after 2 h.

2.4. Reaction of $[\text{Ru}_3(\text{CO})_{12}]$ with 2-ethynylpyridine

A thf solution (15 mL) of $[\text{Ru}_3(\text{CO})_{12}]$ (50 mg, 0.078 mmol) and 2-ethynylpyridine (30 mg, 0.29 mmol) was heated to reflux for

30 min. The solvent was removed under reduced pressure and the residue separated by TLC. Elution with cyclohexane/ CH_2Cl_2 (1 : 2, v/v) developed five bands. The first band was determined to be unreacted $[\text{Ru}_3(\text{CO})_{12}]$ (trace). The second and fifth bands afforded $[\text{Ru}_3(\text{CO})_7(\mu\text{-CO})\{\mu_3\text{-C}_5\text{H}_4\text{NC}=\text{CHC}(\text{C}_5\text{H}_4\text{N})=\text{CH}\}]$ (**5**) (12 mg, 21%) as red crystals and $[\text{Ru}_3(\text{CO})_7(\mu\text{-CO})\{\mu_3\text{-C}_5\text{H}_4\text{-NCCHC}(\text{C}_5\text{H}_4\text{N})\text{CHCHC}(\text{C}_5\text{H}_4\text{N})\}]$ (**6**) (10 mg, 15%) as orange crystals after recrystallization from *n*-hexane/ CH_2Cl_2 at 4 °C. The contents of the other bands were too small for complete characterization. Data for **5**: anal. calc. for $\text{C}_{22}\text{H}_{10}\text{N}_2\text{O}_8\text{Ru}_3$: C, 36.02; H, 1.37; N, 3.82. Found: C, 36.22; H, 1.42; N, 3.90%. IR ($\nu(\text{CO})$, CH_2Cl_2): 2068m, 2039vs, 2014s, 1998m, 1965w, 1937w, 1792w, 1719w cm^{-1} . $^1\text{H NMR}$ (CD_2Cl_2): δ 9.49 (d, J 2.4 Hz, 1H), 8.76 (d, J 5.2 Hz, 1H), 8.62 (d, J 5.2 Hz, 1H), 7.77 (t, J 8.0 Hz, 2H), 7.59 (dd, J 12.0, 8.0 Hz, 2H), 7.29 (t, J 6.0 Hz, 1H), 7.21 (t, J 6.0 Hz, 1H), 6.96 (d, J 2.4 Hz, 1H). Data for **6**: anal. calc. for $\text{C}_{29}\text{H}_{15}\text{N}_3\text{O}_8\text{Ru}_3$: C, 41.63; H, 1.81; N, 5.02. Found: C, 41.88; H, 1.89; N, 5.09%. IR ($\nu(\text{CO})$, CH_2Cl_2): 2091m, 2056vs, 2023m, 1996m, 1985m, 1951w, 1888w cm^{-1} . $^1\text{H NMR}$ (CD_2Cl_2): δ 8.58 (d, J 4.0 Hz, 1H), 8.49 (d, J 4.0 Hz, 1H), 8.12 (m, 2H), 7.85 (m, 1H), 7.77 (m, 2H), 7.68 (m, 2H), 7.61 (m, 1H), 7.23 (t, J 6.0 Hz, 1H),

Table 1 Crystal data and structure refinement details for compounds **1–3**, **5**, and **6**

Compound	1	2	3	5	6
CCDC	2009586	2009587	2009588	2009591	2009592
Empirical formula	$\text{C}_{17}\text{H}_6\text{NO}_{10}\text{Os}_3$	$\text{C}_{16}\text{H}_6\text{NO}_9\text{Os}_3$	$\text{C}_{17.5}\text{H}_5\text{ClNO}_{11}\text{Os}_3$	$\text{C}_{22}\text{H}_{10}\text{N}_2\text{O}_8\text{Ru}_3$	$\text{C}_{29}\text{H}_{15}\text{N}_3\text{O}_8\text{Ru}_3$
Formula weight	954.83	926.82	1011.27	733.53	836.65
Temperature (K)	150(1)	150(1)	193(1)	193(1)	193(1)
Wavelength (Å)	0.71073	0.71073	0.71073	0.71073	0.71073
Crystal system	Triclinic	Monoclinic	Monoclinic	Triclinic	Triclinic
Space group	$P\bar{1}$	$P2_1/n$	C_2/c	$P\bar{1}$	$P\bar{1}$
Unit cell dimensions					
<i>a</i> (Å)	8.7108(4)	8.1249(2)	17.575(4)	8.187(5)	11.114(18)
<i>b</i> (Å)	9.1324(4)	15.2910(4)	8.329(2)	9.641(6)	11.221(17)
<i>c</i> (Å)	14.1005(6)	15.3121(4)	30.267(6)	15.139(9)	13.16(2)
α (°)	100.068(4)	100.068(4)	90	97.65(3)	75.91(5)
β (°)	92.632(4)	91.697(2)	96.45(3)	94.716(17)	73.55(6)
γ (°)	111.204(4)	111.204(4)	90	106.30(2)	61.99(9)
Volume (Å ³)	1022.35(8)	1901.52(8)	4402.6(17)	1127.7(12)	1377(4)
<i>Z</i>	2	4	8	2	2
Density (calculated) (Mg m^{-3})	3.102	3.237	3.051	2.160	2.017
Absorption coefficient (mm^{-1})	18.652	20.047	17.455	2.036	1.682
<i>F</i> (000)	846	1636	3600	704	812
Crystal size (mm^3)	$0.28 \times 0.16 \times 0.10$	$0.18 \times 0.16 \times 0.08$	$0.12 \times 0.11 \times 0.04$	$0.12 \times 0.08 \times 0.03$	$0.25 \times 0.20 \times 0.04$
2θ range for data collection (°)	6.854 to 51.998	6.336 to 53.996	4.664 to 54.482	4.462 to 54.31	4.472 to 54.436
Reflections collected	15 181	30 729	32 329	32 047	31 001
Independent reflections [R_{int}]	4006 [$R_{\text{int}} = 0.0553$]	4142 [$R_{\text{int}} = 0.0623$]	4927 [$R_{\text{int}} = 0.0428$]	5010 [$R_{\text{int}} = 0.0468$]	6101 [$R_{\text{int}} = 0.0720$]
Data/restraints/parameters	4006/0/281	4142/0/270	4927/0/312	5010/0/316	6101/0/388
Goodness-of-fit on F^2	1.017	1.103	1.135	1.039	1.052
Final <i>R</i> indices [$I > 2\sigma(I)$]	$R_1 = 0.0269$, $wR_2 = 0.0623$	$R_1 = 0.0211$, $wR_2 = 0.0459$	$R_1 = 0.0261$, $wR_2 = 0.0534$	$R_1 = 0.0323$, $wR_2 = 0.0775$	$R_1 = 0.0687$, $wR_2 = 0.1619$
<i>R</i> indices (all data)	$R_1 = 0.0294$, $wR_2 = 0.0641$	$R_1 = 0.0239$, $wR_2 = 0.0471$	$R_1 = 0.0318$, $wR_2 = 0.0551$	$R_1 = 0.0497$, $wR_2 = 0.0854$	$R_1 = 0.1010$, $wR_2 = 0.1872$
Largest diff. peak and hole ($\text{e} \text{ \AA}^{-3}$)	2.26/−1.46	1.06/−1.50	1.22/−0.99	1.24/−0.83	3.27/−1.45

7.14 (t, *J* 6.0 Hz, 1H), 6.95 (d, *J* 4.0 Hz, 1H), 6.75 (t, *J* 6.0 Hz, 1H), 4.57 (d, *J* 3.6, 1H).

2.5. Reaction of $[\text{Ru}_3(\text{CO})_{10}(\text{NCMe})_2]$ with 2-ethynylpyridine

To an MeCN solution (20 mL) of $[\text{Ru}_3(\text{CO})_{10}(\text{NCMe})_2]$ (0.15 g, 0.23 mmol) was added 2-ethynylpyridine (47 mg, 0.46 mmol) at -78°C and the reaction mixture was allowed to warm to room temperature. The mixture was further stirred at room temperature for 30 min. The solvent was removed under reduced pressure and the residue chromatographed by TLC on silica gel. Elution with cyclohexane/ CH_2Cl_2 (1 : 1, v/v) developed two bands. The faster-moving band was unreacted $[\text{Ru}_3(\text{CO})_{10}(\text{NCMe})_2]$ (trace), while the slower-moving band afforded **5** (50 mg, 30%).

2.6. Crystal structure determinations

Single crystals of **1–3**, **5**, and **6** suitable for X-ray diffraction analysis were grown by slow diffusion of *n*-hexane into a CH_2Cl_2 solution containing each product. Suitable crystals of **1** and **2** were mounted on an Agilent Super Nova dual diffractometer (Agilent Technologies Inc., Santa Clara, CA) using a Nylon loop and Paratone oil and the diffraction data were collected at 150(1) K using Mo- $K\alpha$ radiation ($\lambda = 0.71073$). Unit cell determination, data reduction, and absorption corrections were carried out using CrysAlisPro.²³ The structures were solved either with the Superflip²⁴ structure solution program using Charge Flipping (for **1**) or with the ShelXS²⁵ structure solution program by direct methods (for **2**) and refined by full-matrix least-squares based on F^2 using ShelXL²⁶ within the OLEX2 (ref. 27) graphical user interface. Suitable crystals of **3**, **5**, and **6** were mounted on a Bruker APEX-III CCD diffractometer using nylon loop and Paratone oil, and the diffraction data were collected at 193(1) K using Mo- $K\alpha$ radiation ($\lambda = 0.71073$). Unit cell determination, data reduction, and absorption corrections were carried out using SAINT software.²⁸ The structures were

solved with the ShelXS²⁵ structure solution program by direct methods and refined by full-matrix least-squares based on F^2 using ShelXL²⁶ within the OLEX2 (ref. 27) graphical user interface. All non-hydrogen atoms were anisotropically refined, while the hydrogen atoms (except those directly bonded to metals) were included using a riding model. The asymmetric unit of **3** also contains part of a CH_2Cl_2 molecule whose carbon atom is disordered and is refined over two sites using 50% occupancy. Pertinent crystallographic parameters are given in Table 1.

2.7. Computational methodology

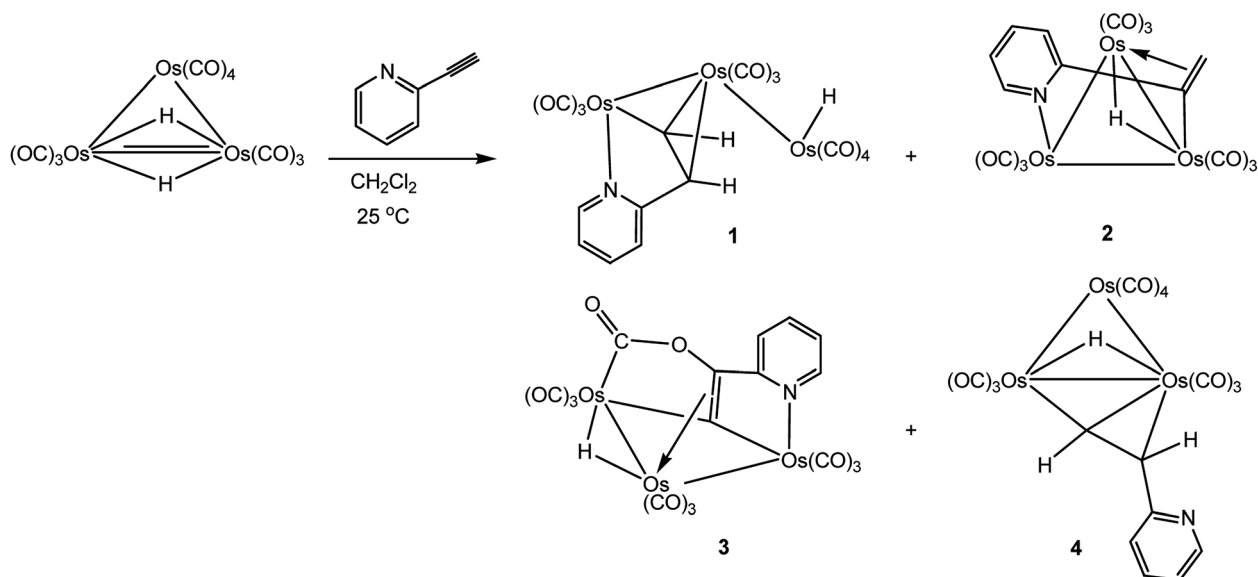
All calculations were performed with the hybrid meta exchange-correlation functional M06,²⁹ as implemented by the Gaussian 09 program package.³⁰ The osmium and ruthenium atoms were described by Stuttgart–Dresden effective core potentials (ECP) and an SDD basis set,³¹ while a 6-31G(d') basis set was employed for the remaining atoms.³² All optimizations were performed using an ultrafine grid and included Grimme's dispersion correction.³³

The reported geometries represent fully optimized ground states (positive eigenvalues) based on the Hessian matrix, and the natural charges (*Q*) and Wiberg bond indices were computed using Weinhold's natural bond orbital (NBO) program (version 3.1).^{34,35} The geometry-optimized structures presented here have been drawn with the JIMP2 molecular visualization and manipulation program.³⁶

3. Results and discussion

3.1. Reaction of $[\text{H}_2\text{Os}_3(\text{CO})_{10}]$ with 2-ethynylpyridine: formation of metalated alkenyl clusters

The reaction between $[\text{H}_2\text{Os}_3(\text{CO})_{10}]$ and a slight excess of 2-ethynylpyridine proceeds rapidly at room temperature with the parent cluster fully consumed in *ca.* 10 min as confirmed by ^1H



Scheme 2 Products **1–4** isolated from the reaction of $[\text{H}_2\text{Os}_3(\text{CO})_{10}]$ with 2-ethynylpyridine.

NMR spectroscopy, which revealed the presence of new hydride resonances at δ -9.82 , -15.79 , -17.72 , and -18.78 . The four products were separated by preparative TLC, and, to our surprise, only three of the four products that were isolated exhibited ^1H NMR data in agreement with the initial reaction mixture. The product hydride at δ -15.79 is unstable and transforms into a new product (band 3) during chromatographic separation. This premise was corroborated by ^1H NMR control experiments that established the stability of the four initial products at room temperature over several days. The products unaffected by chromatography correspond to the first, second, and fourth bands on the TLC plate. Recrystallization attempts to isolate the hydride product associated with the resonance at δ -15.79 were not successful, and we employed chromatography to separate this product from the initial mixture. The products isolated by preparative TLC, in order of elution, were established as $[\text{HOs}_3(\text{CO})_{10}(\mu\text{-C}_5\text{H}_4\text{NCH}=\text{CH})]$ (**1**), $[\text{HOs}_3(\text{CO})_9(\mu_3\text{-C}_5\text{H}_4\text{NC}=\text{CH}_2)]$ (**2**), $[\text{HOs}_3(\text{CO})_9(\mu_3\text{-C}_5\text{H}_4\text{NC}=\text{CCO}_2)]$ (**3**), and $[\text{HOs}_3(\text{CO})_{10}(\mu\text{-CH}=\text{CHC}_5\text{H}_4\text{N})]$ (**4**) in yields of 25, 15, 30, and 20%, respectively (Scheme 2). We repeated the reaction depicted in Scheme 2 several times and confirmed that the distribution of the cluster products is unaffected when the cluster : alkyne ratio was changed from 1 : 2 to 1 : 10. Clusters **1** and **4** represent the two products previously described in the LHD report.¹¹ Performing the reaction at 50 °C in *n*-hexane furnished the same four initial products, but the yield of **4** was greatly reduced. The lability of purified **4** was investigated under comparable conditions and was found to be unstable, transforming to **1** after 2 h at 60 °C. These data indicate that **4** is the product of kinetic substitution with **1** representing the thermodynamically preferred isomer, a feature that was confirmed by DFT calculations (*vide infra*).

The identity of clusters **1**–**4** was examined spectroscopically by IR and NMR, and the molecular structures for clusters **1**–**3** were established by X-ray crystallography. Our product **1** corresponds to the minor product in the LHD report, which incidentally is also labeled as **1** in the original report.¹¹ Given the quality of earlier diffraction data collected for **1** ($R = 0.1001$), we collected a new data set for **1** and re-determined its solid-state structure (Fig. 1). Surprisingly, our structure is

polymorphic to the original LHD structure. As with the original structure, we were unable to locate the terminal hydride ligand on the “spike” $\text{Os}(\text{CO})_4$ moiety. The location of the terminal hydride, while not established in the original report containing **1**, is supported by the ligand distribution at the $\text{Os}(\text{CO})_4$ center in **1**. Moreover, the solid-state structure of the related PMe_2Ph -substituted derivative $[\text{HOs}_3(\text{CO})_9(\text{PMe}_2\text{Ph})(\mu\text{-C}_5\text{H}_4\text{NCH}=\text{CH})]$, whose hydride shares a common site at the pendent osmium center as **1**, was located during data reduction and verified at the “free” site at the $\text{Os}(\text{CO})_3\text{P}$ center.¹¹ Generally speaking, bridging hydrides are preferred at polynuclear clusters.³⁷ The preference of a terminal *versus* an edge-bridging hydride in **1** was computationally verified, as discussed below.

Since the gross structural features of the two structures for **1** are similar, we will limit our structural discussion to a few highlights. The near-linear $\text{Os}(1)\text{--Os}(2)\text{--Os}(3)$ linkage [$159.593(12)^\circ$] confirms the polyhedral expansion of the metallic core and is a common phenomenon in trimetallic clusters with a 50e count.³⁸ The $\text{C}_5\text{H}_4\text{NCH}=\text{CH}$ ligand bridges the $\text{Os}(1)\text{--Os}(2)$ edge regiospecifically by $\mu\text{-C,N}$ coordination with the nitrogen occupying a terminal position on the metallic frame. The metalated C(11) atom and the N(1) donor are located *syn* to each other at the six-coordinate $\text{Os}(1)$ center. The ethenyl moiety produced from the alkyne/ OsH addition process functions as a π donor to $\text{Os}(2)$ as defined by the C(11)– $\text{Os}(2)$ and C(12)– $\text{Os}(2)$ bonds, whose mean distance of 2.285 Å is >0.23 Å longer than the $\text{Os}(1)\text{--C}(11)$ σ bond [2.084(6) Å]. These structural features are typical of clusters containing π,σ -donating ligands. The metalated ethenylpyridine ligand in **1** donates no electrons to the dangling $\text{Os}(3)$ center, which also contains a terminal hydride ligand that resides at the “empty” coordination site *trans* to the O(8)–C(8)– $\text{Os}(3)$ linkage. The two $\text{Os}\text{--Os}$ vectors exhibit a mean distance of 2.8597 Å, with the bridged $\text{Os}(1)\text{--Os}(2)$ bond [2.8248(4) Å] slightly shorter than the non-bridged $\text{Os}(2)\text{--Os}(3)$ edge [2.8945(4) Å]. The terminal hydride was not located during data refinement, but its location at the $\text{Os}(3)$ atom is supported by the arrangement of carbonyls about the $\text{Os}(3)$ center.

The presence of the expected hydride at the $\text{Os}(3)$ atom was verified by DFT calculations with the computed structure for **A**

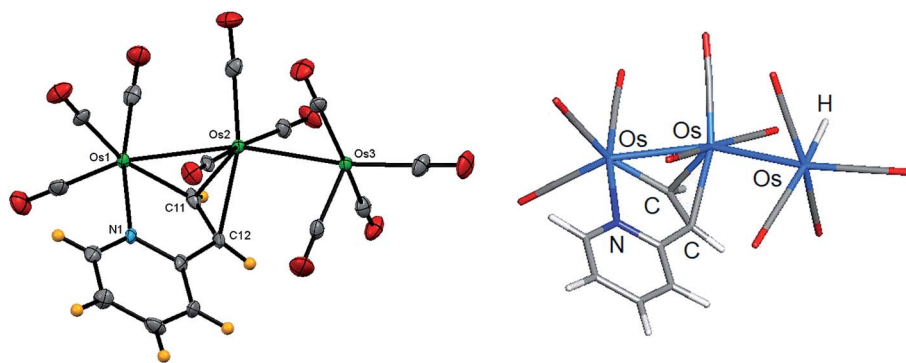


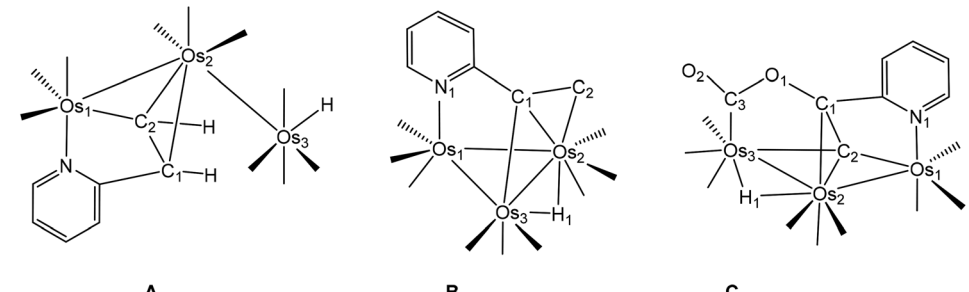
Fig. 1 Solid-state molecular structure of $[\text{HOs}_3(\text{CO})_{10}(\mu\text{-C}_5\text{H}_4\text{NCH}=\text{CH})]$ (**1**, left) showing 50% probability atomic displacement ellipsoids and DFT-optimized structure of **A** (right). Selected bond lengths (Å) and bond angles ($^\circ$) for **1**: $\text{Os}(1)\text{--Os}(2)$ 2.8248(4), $\text{Os}(2)\text{--Os}(3)$ 2.8945(4), $\text{Os}(1)\text{--N}(1)$ 2.144(5), $\text{Os}(1)\text{--C}(11)$ 2.048(6), $\text{Os}(2)\text{--C}(11)$ 2.223(6), $\text{Os}(2)\text{--C}(12)$ 2.346(6), C(11)–C(12) 1.437(9), $\text{Os}(1)\text{--Os}(2)\text{--Os}(3)$ 159.593(12), N(1)– $\text{Os}(1)\text{--Os}(2)$ 83.17(13), N(1)– $\text{Os}(1)\text{--C}(11)$ 78.1(2), $\text{Os}(1)\text{--C}(11)\text{--Os}(2)$ 82.7(2), C(11)– $\text{Os}(2)\text{--C}(12)$ 36.5(2).

depicted in Fig. 1 alongside the experimental structure. Excellent agreement exists between the experimental and the computed structures. The preference for a terminal hydride in **A** versus a bridging hydride at the adjacent Os–Os vector was also examined by DFT through a series of step-scan calculations. Reducing the initial Os–Os–H angle of 83° in species **A** to 25°, well past the typical angle for an edge-bridging hydride of *ca.* 37°, led to an increase in total energy with no sign of a stable stationary point. All attempts to optimize a structure with a bridging hydride collapsed to species **A**, and we confidently estimate an energy difference of ≥ 13 kcal mol⁻¹ in favor of the isomer with a terminal hydride. The natural charges (*Q*) and Wiberg bond indices were also examined, and these data are reported in Table 2. All three osmium atoms exhibit a negative charge that ranges from -0.96 [Os(1)] to -1.55 [Os(3)], as do the

alkenyl carbons C(1) [-0.30] and C(2) [-0.24] and the pyridine N(1) [-0.42] atom. The charge on the terminal H(1) atom is 0.15 and is similar in magnitude to the edge-bridging hydride ligand in species **B** (cluster 2) and **C** (cluster 3). The two Os–Os vectors exhibit a mean Wiberg bond index of 0.35, consistent with their single-bond designation, and the metalated alkenyl moiety displays Wiberg indices of 0.46 and 0.47 for the Os(2)–C(1) and Os(2)–C(2) bonds that are a factor of two weaker than the σ -bonding component defined by the Os(1)–C(2) vector (0.87). Finally, the WBI for the Os(3)–H(1) bond is 0.45.

Whereas the formation of **1** arises from an anti-Markovnikov Os–H/alkyne addition process, cluster **2** derives from a Markovnikov insertion product where the hydride adds to the terminal alkyne carbon to produce a methylene group. The molecular structure of **2** was established by X-ray

Table 2 Natural charges (*Q*) and Wiberg bond indices for the osmium clusters A–C^a



Natural charges (<i>Q</i>)	A	B	C
Os1	-0.96	-1.01	-0.96
Os2	-1.18	-1.24	-1.13
Os3	-1.55	-1.21	-1.29
N1	-0.42	-0.40	-0.41
C1	-0.30	-0.14	0.23
C2	-0.24	-0.39	-0.15
C3			0.75
H1	0.15	0.14	0.13
WBI	A	B	C
Os1–Os2	0.38	0.42	0.37
Os1–Os3		0.48	
Os2–Os3	0.31	0.30	0.23
Os1–N1	0.52	0.48	0.52
Os1–C2	0.87		0.81
Os2–C1	0.46	0.43	0.42
Os2–C2	0.47	0.44	0.50
Os3–C1		0.67	
Os3–C2			0.74
Os3–C3			0.77
O1–C1			0.92
O1–C3			0.89
O2–C3			1.81
Os1–H1			
Os2–H1		0.42	0.23
Os3–H1	0.45	0.35	0.41

^a Atom numbering for the participant atoms follows the structures depicted below the table caption.

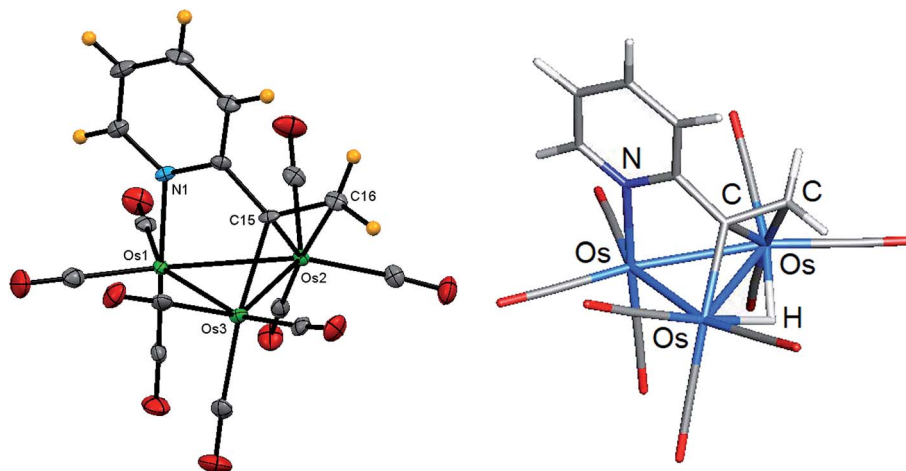


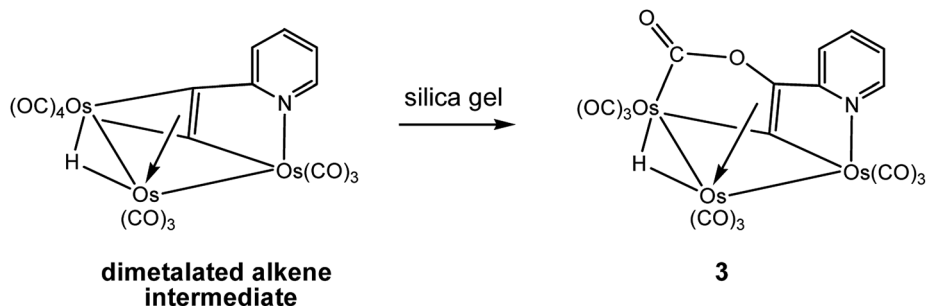
Fig. 2 Solid-state molecular structure of $[\text{HOs}_3(\text{CO})_9(\mu_3\text{-C}_5\text{H}_4\text{NC}=\text{CH}_2)]$ (**2**, left) showing 50% probability atomic displacement ellipsoids and DFT-optimized structure of **B** (right). Selected bond lengths (Å) and bond angles ($^\circ$) for **2**: Os(1)–Os(2) 2.8576(3), Os(2)–Os(3) 2.8581(2), Os(1)–Os(3) 2.7913(3), Os(1)–N(1) 2.162(4), Os(2)–C(15) 2.242(4), Os(2)–C(16) 2.306(5), Os(3)–C(15) 2.122(4), C(15)–C(16) 1.393(7), N(1)–Os(1)–Os(2) 86.03(10), N(1)–Os(1)–Os(3) 85.64(10), C(15)–Os(3)–Os(2) 50.93(12), Os(2)–C(15)–Os(3) 81.78(15), C(15)–Os(2)–C(16) 35.63(17).

crystallography, and the solid-state structure is shown in Fig. 2. The cluster core contains a closed osmium triangle where the Os–Os bond distances range from 2.7913(3) Å [Os(1)–Os(3)] to 2.8581(2) Å [Os(2)–Os(3)] with a mean distance of 2.8357 Å. Each osmium is bound to three carbonyls, and the 5e donor $\text{C}_5\text{H}_4\text{NC}=\text{CH}_2$ caps a metallic face through the N(1), C(15), and C(16) atoms. The Os(2) and Os(3) centers bind the latter two atoms of the ligand in a traditional σ, π -vinyl fashion, with the Os(3)–C(15) bond representing the σ component of the metallated alkenyl moiety. The longer Os(2)–C(15) [2.242(4) Å] and Os(2)–C(16) [2.306(5) Å] bonds represent the π component of this ligand, whose Os–C distances are comparable to those bond distances reported in related clusters.^{11,18,20} The hydride was not located during data reduction but was assumed to span the Os(2)–Os(3) edge based on the disposition of CO ligands about the Os–Os bond. The locus for the hydride was subsequently verified by DFT calculations, and the optimized structure is depicted alongside the experimental structure in Fig. 2. The optimized structure of **B** closely mirrors the experimental structure with the bridging hydride sharing the Os(2)–Os(3) vector bridged by the alkenyl ligand. The hydride is tipped slightly below the metallic plane opposite the polyhedral face capped by the $\text{C}_5\text{H}_4\text{NC}=\text{CH}_2$ ligand. The osmium atoms and

the Os-bound N(1), C(1), and C(2) atoms of the activated ligand all display a negative charge, while the edge-bridging hydride exhibits a positive charge of 0.14. The computed WBI for the Os–Os bonds in **B** range from 0.30 [Os(2)–Os(3)] to 0.48 [Os(1)–Os(2)] with a mean index of 0.40. The Os–N and Os–C WBIs in **B** associated with the capping $\text{C}_5\text{H}_4\text{NC}=\text{CH}_2$ ligand parallel those data reported for **A**. Finally, the Os–H bond indices for the edge-bridging hydride are comparable in magnitude to the WBIs in related hydride clusters investigated by us.³⁹

The spectroscopic properties of **2** are consistent with the solid-state structure. The ^1H NMR spectrum reveals a pair of doublets at δ 8.56 (J 6.0 Hz) and δ 6.92 (J 8.0 Hz) and a pair of multiplets at δ 7.64 and δ 6.98 that are readily ascribed to the ABCD spin system of the pyridyl ring. The two singlets are δ 4.30 and 2.63 are assigned to the hydrogens of the vinyl moiety, with the lower-field singlet confidently assigned to the hydrogen situated syn to the hydride ligand (δ –17.70) based on NOESY ^1H NMR experiments.

Recall, one of the four initial products produced in the reaction between $[\text{H}_2\text{Os}_3(\text{CO})_{10}]$ and 2-ethynylpyridine is not stable over silica gel, transforming to cluster **3** during chromatographic separation. The hydride signal for the intermediate appears at δ –15.79 and it shifts 0.97 ppm upfield after



Scheme 3 SiO_2 -promoted conversion of the proposed alkenyl-substituted intermediate to **3**.

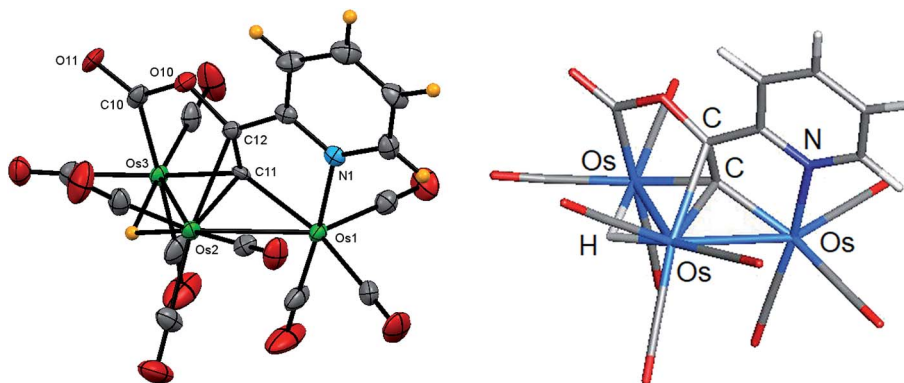


Fig. 3 Solid-state molecular structure of $[\text{HOs}_3(\text{CO})_9(\mu_3\text{-C}_5\text{H}_4\text{NC}=\text{CCO}_2)]$ (**3**, left) showing 50% probability atomic displacement ellipsoids and DFT-optimized structure of **C** (right). Selected bond lengths (Å) and bond angles ($^\circ$) for **3**: Os(1)–Os(2) 2.8464(9), Os(2)–Os(3) 2.9561(10), Os(1)–N(1) 2.137(5), Os(1)–C(11) 2.076(5), Os(2)–C(11) 2.171(5), Os(2)–C(12) 2.301(6), Os(3)–C(10) 2.101(6), Os(3)–C(11) 2.079(5), C(11)–C(12) 1.410(8), Os(1)–Os(2)–Os(3) 83.83(2), N(1)–Os(1)–Os(2) 84.82(13), C(10)–Os(3)–Os(2) 80.57(15), C(11)–Os(2)–C(12) 36.6(2).

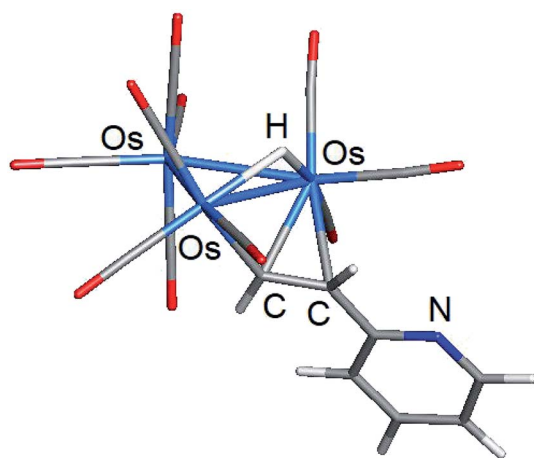
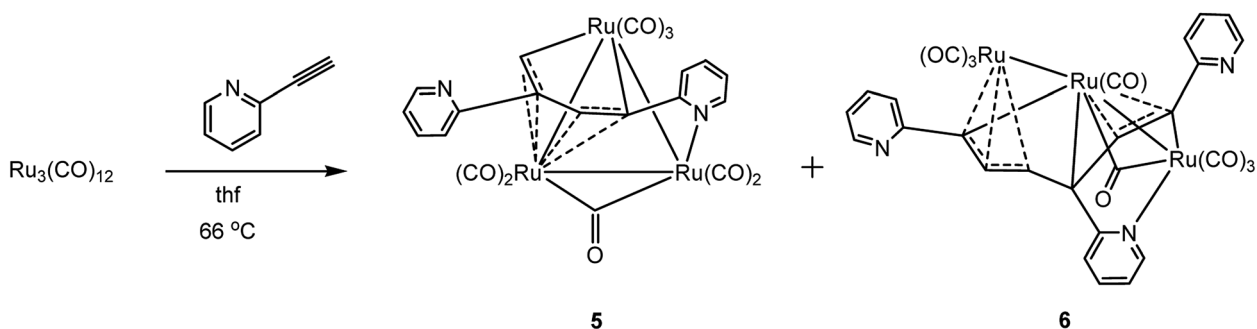


Fig. 4 DFT-optimized structure of major product **A_{alt}** from the room temperature reaction of $[\text{H}_2\text{Os}_3(\text{CO})_{10}]$ and 2-ethynylpyridine.

chromatography. We had to settle on the characterization of this unknown intermediate using isolated **3**. NMR analysis of the crude reaction mixture suggests that the silica gel-unstable intermediate does not contain any vinyl hydrogens, leading us to propose the transformation depicted in Scheme 3 as an explanation of the precursor to **3**. Here the dimetalated alkenyl

moiety of the intermediate undergoes ring expansion through an oxygen capture pathway that is assisted by an ancillary CO ligand at the $\text{Os}(\text{CO})_4$ center. No change in the initial product mixture was observed over several hours when exposed to oxygen, suggesting that the stationary support serves as the source of oxygen in this reaction.

Fig. 3 shows the solid-state molecular structure of **3** with selected bond distances and angles reported in the caption. The molecule contains 50e, assuming the face-capping $\text{C}_5\text{H}_4\text{NC}=\text{CCO}_2$ ligand functions as a 7e donor, and the opened triosmium core is in concert with the overall electron count.³⁸ The Os(1)–Os(2) [2.8464(9) Å] and Os(2)–Os(3) [2.9561(10) Å] bond distances are consistent with their single-bond designation and the Os–Os bond distances in clusters **1** and **2**. Each metal center contains three terminal CO ligands that are situated at mutually *cis* sites to furnish $\text{Os}(\text{CO})_3$ units possessing one axial and two equatorial CO groups. The hydride, which was located crystallographically, spans the Os(2)–Os(3) edge, which is significantly longer (*ca.* 0.1 Å) than the non-hydride bridged Os(1)–Os(2) vector. The $\text{C}_5\text{H}_4\text{NC}=\text{CCO}_2$ ligand may be viewed as a doubly metalated σ, σ, π -alkenyl ligand with the Os(1)–C(11) and Os(3)–C(11) bonds corresponding to the σ components and the π bond represented by the Os(2)–C(11) and Os(2)–C(12) bonds. The mean distance of 2.078 Å for the former two Os–C bonds is *ca.* 0.16 Å shorter than the mean distance displayed by the latter



Scheme 4 Reaction of $[\text{Ru}_3(\text{CO})_{12}]$ with 2-ethynylpyridine.

two Os–C(π) bonds of the alkenyl linkage. The carboxylate ligand, which is defined by the C(10), O(10), and O(11) atoms, exhibits bond distances and angles that are unremarkable and require no comment. The presence of the carboxylate group in **3** was supported by IR spectroscopy based on a low-energy $\nu(\text{CO})$ band at 1693 cm^{-1} . The optimized structure of **C** is depicted alongside the experimental structure, and excellent agreement between the two structures is noted. Apart from the positive charge of 0.23 computed for the C(1) atom of alkenyl ligand, whose adjacent O(1) atom likely serves to withdraw electron density for the metalated carbon center, the charges and WBIs for **C** mirror the data reported for species **A** and **B**.

The slowest moving band isolated from the TLC plate was confirmed as cluster **4**, and this material corresponds to the major product reported in the LHD study.¹¹ The initial identity of this product was formulated based on the solution spectroscopic data. The ^1H NMR spectrum supported a product with a single hydride and *trans* alkenyl moiety while the IR spectrum was consistent with a triangular cluster having ten terminal CO ligands. These data supported a product involving the addition of the Os–H bond to the alkyne triple bond. The ancillary pyridyl ligand remains free and functions as a non-coordinated spectator ligand. Accordingly, the product was formulated as possessing a structure similar to the known vinyl cluster $[\text{H}_2\text{Os}_3(\text{CO})_{10}(\mu, \eta^2\text{-CH}=\text{CH}_2)]$,⁴⁰ as depicted by the major product in Scheme 1.

As with the earlier LHD study, we were unable to grow X-ray quality crystals of this product and could not unequivocally establish its molecular structure. Accordingly, we examined the LHD-proposed structure of **4** (species **A**_{alt}) by electronic structure calculations [Fig. 4]. Both the hydride and alkenyl moiety share the same edge of the Os_3 polyhedron. Species **A** and **A**_{alt} are isomers, and the former is computed to be 8.9 kcal mol^{-1} (ΔG) more stable. Independent control experiments confirmed **4** (kinetic isomer) as the precursor to **1** (thermodynamic isomer). Repeating the reaction between $[\text{H}_2\text{Os}_3(\text{CO})_{10}]$ and 2-ethynylpyridine in refluxing hexane furnished cluster **1** at the expense of cluster **4**. The yields of **2** and **3** remained unchanged. Heating pure **4** in CDCl_3 in a sealed NMR

tube at $60\text{ }^\circ\text{C}$ led to the conversion to **1** after 2 h, confirming cluster **1** as the thermodynamically preferred isomer. We also examined the transformation of **4** \rightarrow **1** at $100\text{ }^\circ\text{C}$ in toluene- d_8 , but the reaction was accompanied by visible cluster decomposition. Subsequent studies confirmed that cluster **1** is unstable at $100\text{ }^\circ\text{C}$.

3.2. Reactions of $[\text{Ru}_3(\text{CO})_{12-n}(\text{NCMe})_n]$ ($n = 0, 2$) with 2-ethynylpyridine: C–C bond formation

The reaction between $[\text{Ru}_3(\text{CO})_{12}]$ and 2-ethynylpyridine follows a different pathway compared to the reactivity described for $[\text{H}_2\text{Os}_3(\text{CO})_{10}]$. The dominant manifolds in the reaction of $[\text{Os}_3(\text{CO})_{10}(\mu\text{-H})_2]$ with 2-ethynylpyridine involve hydride transfer to the alkyne moiety and C–H bond activation of the alkyne functionality. The reaction of $[\text{Ru}_3(\text{CO})_{12}]$ with excess 2-ethynylpyridine is dominated by C–C bond coupling of the alkyne moiety of 2-ethynylpyridine to furnish $[\text{Ru}_3(\text{CO})_7(\mu\text{-CO})\{\mu_3\text{-C}_5\text{H}_4\text{NC}=\text{CHC}(\text{C}_5\text{H}_4\text{N})=\text{CH}\}]$ (**5**) and $[\text{Ru}_3(\text{CO})_7(\mu\text{-CO})\{\mu_3\text{-C}_5\text{H}_4\text{NCCHC}(\text{C}_5\text{H}_4\text{N})\text{CHCHC}(\text{C}_5\text{H}_4\text{N})\}]$ (**6**) in 21 and 15% yield, respectively (Scheme 4). Cluster **5** does not serve as a precursor to **6** since control experiments in refluxing thf confirmed that **5** was inert to further 2-ethynylpyridine insertion. In an attempt to isolate a ruthenium cluster with a single metalated 2-ethynylpyridine ligand, we also treated $[\text{Ru}_3(\text{CO})_{10}(\text{NCMe})_2]$ with two equivalents of 2-ethynylpyridine at ambient temperature, but this reaction afforded only **5** in 30% yield. The two products were separated by chromatography and characterized by solution methods (IR and NMR) and each molecular structure established by X-ray crystallography.

The solid-state molecular structure of **5** is depicted in Fig. 5 along with selected bond distances and angles contained in the figure caption. The triangular Ru_3 cluster is ligated by seven terminal carbonyls, an edge-bridging carbonyl, and a $\mu_3\text{-C}_5\text{H}_4\text{NC}=\text{CHC}(\text{C}_5\text{H}_4\text{N})=\text{CH}$ ligand. The Ru–Ru distances range between 2.7868(15) and 2.8747(15) Å with the Ru(2)–Ru(3) edge, which accommodates the bridging carbonyl ligand, being the longest of the three Ru–Ru bonds. The $\text{C}_5\text{H}_4\text{NC}=\text{CHC}(\text{C}_5\text{H}_4\text{N})=\text{CH}$ ligand, which is formed *via* head-to-tail C–C coupling of the ethynyl moieties, functions as an 8e donor

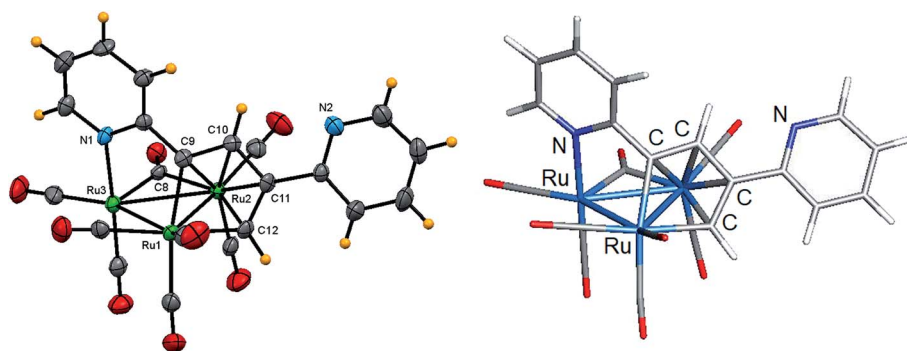
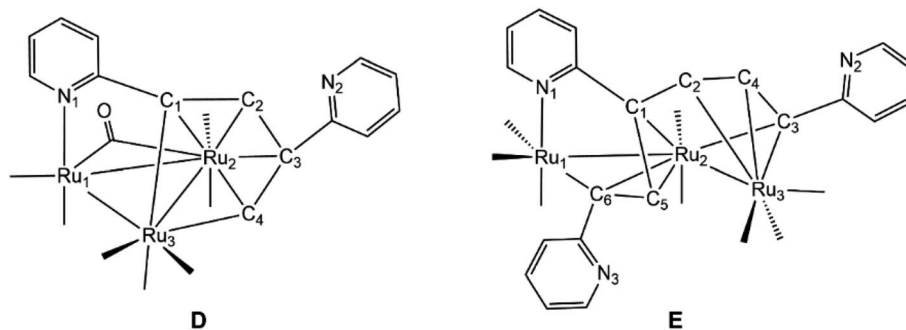


Fig. 5 Solid-state molecular structure of $[\text{Ru}_3(\text{CO})_7(\mu\text{-CO})\{\mu_3\text{-C}_5\text{H}_4\text{NC}=\text{CHC}(\text{C}_5\text{H}_4\text{N})=\text{CH}\}]$ (**5**, left) showing 50% probability atomic displacement ellipsoids and DFT-optimized structure of **D** (right). Selected bond lengths (Å) and bond angles ($^\circ$) for **5**: Ru(1)–Ru(2) 2.7868(15), Ru(2)–Ru(3) 2.8747(15), Ru(1)–Ru(3) 2.8426(16), Ru(3)–N(1) 2.150(4), Ru(1)–C(9) 2.081(4), Ru(1)–C(12) 2.066(4), Ru(2)–C(9) 2.279(4), Ru(2)–C(10) 2.241(4), Ru(2)–C(11) 2.250(4), Ru(2)–C(12) 2.233(4), Ru(2)–C(8) 2.137(4), Ru(3)–C(8) 1.980(4), C(9)–C(10) 1.391(5), C(10)–C(11) 1.450(5), C(11)–C(12) 1.398(6), N(1)–Ru(3)–Ru(1) 84.58(9), N(1)–Ru(3)–Ru(2) 89.28(9), Ru(2)–C(8)–Ru(3) 88.49(16).

ligand that is best viewed as a dimetalated 2-pyridyl-substituted butadiene ligand. The Ru(1)–C(9) and Ru(1)–C(12) vectors, which represent the two metalated bonds associated with the ruthenacyclopentadiene ring defined by the Ru(1)–C(9)–C(10)–C(11)–C(12) atoms, display a mean distance of 2.074 Å. This ligand donates an additional four electrons to the Ru(2) center *via* the butadiene component of the ruthenacyclopentadiene ring and two electrons through coordination of the pyridyl N(1) moiety to the Ru(3) center. The Ru(3)–N(1) [2.150(4) Å] bond distance and the Ru–C bond distances for the coordinated butadiene moiety [Ru(1)–C(9) 2.081(4), Ru(1)–C(12) 2.066(4),

Ru(2)–C(9) 2.279(4), Ru(2)–C(10) 2.241(4), Ru(2)–C(11) 2.250(4), Ru(2)–C(12) 2.233(4) Å] are similar to those distances found in related clusters.^{17,20} The cluster is electronically saturated based on an electron count of 48e, and the optimized structure of **D** (Fig. 5) mirrors the experimental structure. Table 3 reports the natural charges and Wiberg bond indices for **D**. The three rutheniums, the two nitrogens, and the coordinated carbon atoms of the butadiene moiety of the μ_3 -C₅H₄NC=CHC(C₅H₄-N)=CH ligand all exhibit a negative charge. The metalated Ru(3)–C(1) and Ru(3)–C(4) bonds of the ligand display a mean WBI of 0.72 that is twofold stronger than the mean WBI index of

Table 3 Natural charges (*Q*) and Wiberg bond indices for the ruthenium clusters **D** and **E**^a



Natural charges (<i>Q</i>)	D	E
Ru1	−0.85	−1.09
Ru2	−0.98	−0.84
Ru3	−1.27	−1.11
N1	−0.41	−0.41
N2	−0.49	−0.48
N3		−0.48
C1	−0.07	−0.16
C2	−0.16	−0.27
C3	−0.04	−0.06
C4	−0.18	−0.12
C5		−0.12
C6		−0.09
WBI	D	E
Ru1–Ru2	0.29	0.32
Ru1–Ru3	0.24	
Ru2–Ru3	0.30	0.40
Ru1–N1	0.43	0.47
Ru1–C6		0.71
Ru2–C1	0.38	0.48
Ru2–C2	0.31	
Ru2–C3	0.28	0.65
Ru2–C4	0.41	
Ru2–C5		0.22
Ru2–C6		0.37
Ru3–C1	0.68	
Ru3–C2		0.50
Ru3–C3		0.53
Ru3–C4	0.75	0.30

^a Atom numbering for the participant atoms follows the structures depicted below the table caption.

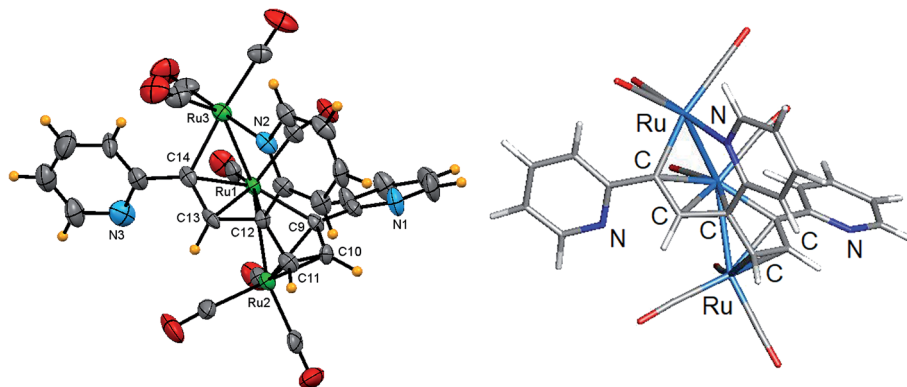


Fig. 6 Solid-state molecular structure of $[\text{Ru}_3(\text{CO})_7(\mu\text{-CO})\{\mu_3\text{-C}_5\text{H}_4\text{NCCHC}(\text{C}_5\text{H}_4\text{N})\text{CHCHC}(\text{C}_5\text{H}_4\text{N})\}]$ (**6**, left) showing 50% probability atomic displacement ellipsoids and DFT-optimized structure of **E** (right). Selected bond lengths (Å) and bond angles ($^\circ$) for **6**: Ru(1)–Ru(2) 2.764(4), Ru(1)–Ru(3) 2.774(3), Ru(3)–N(2) 2.138(9), Ru(1)–C(9) 2.093(10), Ru(1)–C(12) 2.146(9), Ru(1)–C(13) 2.270(9), Ru(1)–C(14) 2.291(9), Ru(2)–C(9) 2.154(9), Ru(2)–C(10) 2.189(9), Ru(2)–C(11) 2.249(10), Ru(3)–C(14) 2.079(10), Ru(1)–C(1) 1.905(10), Ru(3)–C(1) 2.541(10), C(9)–C(10) 1.417(13), C(10)–C(11) 1.428(13), C(11)–C(12) 1.465(13), C(12)–C(13) 1.480(12), C(13)–C(14) 1.405(14), Ru(2)–Ru(1)–Ru(3) 152.05(6), N(2)–Ru(3)–Ru(1) 84.4(2), N(2)–Ru(3)–C(14) 90.1(4), Ru(1)–C(1)–O(1) 159.5(9), Ru(3)–C(1)–O(1) 123.7(7).

0.36 for the Ru(2)–C(π) bonds involving C(1)–C(4) atoms of the butadiene moiety. Finally, the solution spectroscopic data for **5** also support the solid-state structure. The IR spectrum exhibits seven carbonyl stretching bands between 2068–1937 cm^{-1} for the terminal carbonyls along with a low-energy absorption at 1792 cm^{-1} assigned to the bridging carbonyl ligand. The ^1H NMR spectrum displays a series of pyridyl multiplets and alkenyl protons consistent with the solid-state structure.

Fig. 6 shows the solid-state molecular structure of **6** and the caption contains selected bond distances and angles. The cluster contains 50-valence electrons and exhibits an expanded triruthenium core that possesses two formal Ru–Ru bonds. The coordination sphere of **6** contains eight carbonyl groups and a $\text{C}_5\text{H}_4\text{NCCHC}(\text{C}_5\text{H}_4\text{N})\text{CHCHC}(\text{C}_5\text{H}_4\text{N})$ ligand, the latter which is formed *via* alkyne C–C bond coupling of three 2-ethynylpyridine ligands. The alkyne-based ligand functions as a 10e donor and may be considered as a dimetalated tris(2-pyridyl-substituted) conjugated triene ligand. The two Ru–Ru bonds defined by the Ru(1)–Ru(2) and Ru(1)–Ru(3) vectors exhibit a mean distance of 2.769 Å that is similar in magnitude to the shortest Ru–Ru bond distance observed in **5**. Each terminal ruthenium is bound to three carbonyls, while the central ruthenium is bound to two carbonyls, one of which is nominally semibridging in nature based on a bond angle of 159.5(9) $^\circ$ for the Ru(1)–C(1)–O(1) linkage. The dimetalated tris(pyridyl-substituted) triene ligand coordinates all three ruthenium atoms using the alkenyl carbons (σ and π fashion) and one of the pyridyl nitrogens [Ru(3)–N(2)]. The triene moiety displays an altered C–C backbone [C(9)–C(10) 1.417(13), C(10)–C(11) 1.428(13), C(11)–C(12) 1.465(13), C(12)–C(13) 1.480(12), C(13)–C(14) 1.405(14) Å] that effectively transforms the three C=C π units into a discrete pair of 3e donating allyl ligands that bind the Ru(1) and Ru(2) atoms. The metalated components of the ligand are represented by the Ru(1)–C(9) and Ru(3)–C(14) vectors, which display a mean bond distance of 2.086 Å. The Ru(3)–N(2) [2.138(9) Å] and Ru–C(triene) [Ru(1)–C(9) 2.093(10), Ru(1)–C(12) 2.146(9), Ru(1)–C(13) 2.270(9), Ru(1)–C(14)

2.291(9), Ru(2)–C(9) 2.154(9), Ru(2)–C(10) 2.189(9), Ru(2)–C(11) 2.249(10), Ru(3)–C(14) 2.079(10) Å] bond distances involving this ligand are similar to the bond distances in **5** and related ruthenium clusters.^{17,20} The optimized structure of **E** is shown alongside the crystallographic structure in Fig. 6. The computed charges and bond indices for **E** parallel the data reported for **D**.

4. Conclusions

The reactivity of 2-ethynylpyridine at trisruthenium and triruthenium centers has been investigated, and we have isolated and characterized four new trimetallic clusters. The reaction of $[\text{H}_2\text{Os}_3(\text{CO})_{10}]$ with excess 2-ethynylpyridine furnished the new trisruthenium clusters $[\text{HOS}_3(\text{CO})_9(\mu_3\text{-C}_5\text{H}_4\text{NC}=\text{CH}_2)]$ (**2**) and $[\text{HOS}_3(\text{CO})_9(\mu_3\text{-C}_5\text{H}_4\text{NC}=\text{CCO}_2)]$ (**3**) along with the previously reported clusters $[\text{HOS}_3(\text{CO})_{10}(\mu\text{-C}_5\text{H}_4\text{NCH}=\text{CH})]$ (**1**) and $[\text{HOS}_3(\text{CO})_{10}(\mu\text{-CH}=\text{CHC}_5\text{H}_4\text{N})]$ (**4**).¹¹ Cluster **4** transforms into **1** at elevated temperature, confirming the former as the kinetic product of substitution. Clusters **1**, **2**, and **4** are apparently formed by the addition of an Os–H bond across C \equiv C bond of 2-ethynylpyridine, whereas **3** is formed *via* C–H bond activation of the alkyne functionality of 2-ethynylpyridine through an unstable intermediate that affords **3** on chromatographic work-up. In contrast, the reaction between $[\text{Ru}_3(\text{CO})_{12}]$ and 2-ethynylpyridine affords $[\text{Ru}_3(\text{CO})_7(\mu\text{-CO})(\mu_3\text{-C}_5\text{H}_4\text{NC}=\text{CHC}(\text{C}_5\text{H}_4\text{N})=\text{CH})]$ (**5**) and $[\text{Ru}_3(\text{CO})_7(\mu\text{-CO})(\mu_3\text{-C}_5\text{H}_4\text{NCCHC}(\text{C}_5\text{H}_4\text{N})\text{CHCHC}(\text{C}_5\text{H}_4\text{N}))]$ (**6**) *via* C–C coupling of the alkyne moiety of 2-ethynylpyridine at ruthenium centers.

Conflicts of interest

There are no conflicts to declare.

Acknowledgements

Financial support from the Ministry of Science and Technology, the Government of the People's Republic of Bangladesh (SG and SEK) and the Robert A. Welch Foundation (Grant B-1093-MGR)

are acknowledged. The DFT calculations were performed at UNT through CASCaM, which is an NSF-supported facility (CHE-1531468).

References

- 1 L. Zhang, L. Dang, T. B. Wen, H. H.-Y. Sung, I. D. Williams, Z. Lin and G. Jia, *Organometallics*, 2007, **26**, 2849–2860.
- 2 A. G. Wong-Foy, L. M. Henling, M. Day, J. A. Labinger and J. E. Bercaw, *J. Mol. Catal. A: Chem.*, 2002, **189**, 3–16.
- 3 J. Navarro, E. Sola, M. Martín, I. T. Dobrinovitch, F. J. Lahoz and L. A. Oro, *Organometallics*, 2004, **23**, 1908–1917.
- 4 H.-F. Klein, S. Camadanli, R. Beck, D. Leukel and U. Flörke, *Angew. Chem., Int. Ed.*, 2005, **44**, 975–977.
- 5 O. V. Ozerov, M. Pink, L. A. Watson and K. G. Caulton, *J. Am. Chem. Soc.*, 2004, **126**, 2105–2113.
- 6 M. L. Buil, M. A. Esteruelas, E. Goni, M. Oliván and E. Oñate, *Organometallics*, 2006, **25**, 3076–3083.
- 7 J. N. Coalter III, W. E. Streib and K. G. Caulton, *Inorg. Chem.*, 2000, **39**, 3749–3756.
- 8 P. Barrio, M. A. Esteruelas and E. Oñate, *Organometallics*, 2004, **23**, 3627–3639.
- 9 M. A. Esteruelas, F. J. Fernández-Alvarez, M. Oliván and E. Oñate, *J. Am. Chem. Soc.*, 2006, **128**, 4596–4597.
- 10 B. Eguillor, M. A. Esteruelas, M. Oliván and E. Oñate, *Organometallics*, 2005, **24**, 1428–1438.
- 11 K. Burgess, H. D. Holden, B. F. G. Johnson, J. Lewis, M. B. Hursthouse, N. P. C. Walker, A. J. Deeming, P. J. Manning and R. Peters, *J. Chem. Soc., Dalton Trans.*, 1985, 85–90.
- 12 W.-Y. Wong and W.-T. Wong, *J. Organomet. Chem.*, 1996, **513**, 27–29.
- 13 J. P.-K. Lau and W.-T. Wong, *Inorg. Chem. Commun.*, 2003, **6**, 174–177.
- 14 S. Chan, W.-Y. Wong and W.-T. Wong, *J. Organomet. Chem.*, 1994, **474**, C30–C33.
- 15 W.-Y. Wong, S. Chan and W.-T. Wong, *J. Organomet. Chem.*, 1995, **493**, 229–237.
- 16 S. E. Kabir, F. Ahmed, A. Das, M. R. Hassan, D. T. Haworth, S. V. Lindeman, G. M. G. Hossain, T. A. Siddiquee and D. W. Bennett, *J. Organomet. Chem.*, 2008, **693**, 1696–1702.
- 17 K. A. Azam, D. W. Bennett, M. R. Hassan, D. T. Haworth, G. Hogarth, S. E. Kabir, S. V. Lindeman, L. Salassa, S. R. Simi and T. A. Siddiquee, *Organometallics*, 2008, **27**, 5163–5166.
- 18 M. R. Al-Mamun, S. Ghosh, S. E. Kabir and G. Hogarth, *J. Organomet. Chem.*, 2017, **849–850**, 80–87.
- 19 R. H. Naulty, M. P. Cifuentes, M. G. Humphrey, S. Houbrechts, C. Boutton, A. Persoons, G. A. Heath, D. C. R. Hockless, B. Luther-Davies and M. Samoc, *J. Chem. Soc., Dalton Trans.*, 1997, 4167–4174.
- 20 M. M. Hossain, N. Akter, S. Ghosh, V. N. Nesterov, M. G. Richmond, G. Hogarth and S. E. Kabir, *RSC Adv.*, 2019, **9**, 21025–21030.
- 21 E. Sappa and M. Valle, *Inorg. Synth.*, 1977, **26**, 365–369.
- 22 G. A. Foulds, B. F. G. Johnson and J. Lewis, *J. Organomet. Chem.*, 1985, **296**, 147–153.
- 23 *CrysAlisPro; Oxford Diffraction*, Yarnton, England, 2015.
- 24 (a) L. Palatinus and G. Chapuis, *J. Appl. Crystallogr.*, 2007, **40**, 786–790; (b) L. Palatinus and A. van der Lee, *J. Appl. Crystallogr.*, 2008, **41**, 975–984; (c) L. Palatinus, S. J. Prathapa and S. van Smaalen, *J. Appl. Crystallogr.*, 2012, **45**, 575–580.
- 25 G. M. Sheldrick, *Acta Crystallogr., Sect. A: Found. Crystallogr.*, 2008, **64**, 112–122.
- 26 G. M. Sheldrick, *Acta Crystallogr., Sect. C: Struct. Chem.*, 2015, **71**, 3–8.
- 27 O. V. Dolomanov, L. J. Bourhis, R. J. Gildea, J. A. K. Howard and H. Puschmann, *J. Appl. Crystallogr.*, 2009, **42**, 339–341.
- 28 *SAINT Version 8.37*, Bruker AXS, Inc., Madison, WI, 2015.
- 29 Y. Zhao and D. G. Truhlar, *Theor. Chem. Acc.*, 2008, **120**, 215–241.
- 30 M. J. Frisch *et al.*, *Gaussian 09, Revision E.01*, Gaussian, Inc., Wallingford, CT, USA, 2009.
- 31 D. Andrae, U. Haeussermann, M. Dolg, H. Stoll and H. Preuss, *Theor. Chim. Acta*, 1990, **77**, 123–141.
- 32 (a) G. A. Petersson, A. Bennett, T. G. Tensfeldt, M. A. Al-Laham, W. A. Shirley and J. Mantzaris, *J. Chem. Phys.*, 1988, **89**, 2193–2218; (b) G. A. Petersson and M. A. Al-Laham, *J. Chem. Phys.*, 1991, **94**, 6081–6090.
- 33 S. Grimme, S. Ehrlich and L. Goerigk, *J. Comput. Chem.*, 2011, **32**, 1456–1465.
- 34 A. E. Reed, L. A. Curtiss and F. Weinhold, *Chem. Rev.*, 1988, **88**, 899–926.
- 35 K. B. Wiberg, *Tetrahedron*, 1968, **24**, 1083–1096.
- 36 (a) JIMP2, version 0.091, a free program for the visualization and manipulation of molecules: M. B. Hall and R. F. Fenske, *Inorg. Chem.*, 1972, **11**, 768–775; (b) J. Manson, C. E. Webster and M. B. Hall, Texas A&M University, College Station, TX, 2006, <http://www.chem.tamu.edu/jimp2/index.html>.
- 37 D. M. P. Mingos and D. J. Wales, *Introduction to Cluster Chemistry*, Prentice-Hall, Englewood Cliffs, NJ, 1990.
- 38 D. M. P. Mingos, *Acc. Chem. Res.*, 1984, **17**, 311–319.
- 39 N. C. Bhoumik, M. T. R. Joy, S. Ghosh, M. G. Richmond and S. E. Kabir, *Inorg. Chim. Acta*, 2020, **510**, 119733 and references therein.
- 40 (a) A. J. Deeming, S. Hasso and M. Underhill, *Dalton Trans.*, 1975, 1614–1620; (b) J. B. Keister and J. R. Shapley, *J. Organomet. Chem.*, 1975, **85**, C29–C31; (c) E. C. Bryan, B. F. G. Johnson and J. Lewis, *Dalton Trans.*, 1977, 1328–1330; (d) A. G. Orpen, A. V. Rivera, E. G. Bryan, D. Pippard, G. M. Sheldrick and K. D. Rouse, *Chem. Commun.*, 1978, 723–724.